

Fast One-Stage Unsupervised Domain Adaptive Person Search

Tianxiang Cui¹, Huibing Wang^{1*}, Jinjia Peng², Ruoxi Deng³, Xianping Fu¹, Yang Wang^{4*}

¹The College of Information and Science Technology, Dalian Maritime University, China

²The College School of Cyber Security and Computer, Hebei University, China

³The College of Computer Science and Artificial Intelligence, Wenzhou University, China

⁴Key Laboratory of Knowledge Engineering with Big Data, Hefei University of Technology, China

cuitianxiang1@gmail.com, {huibing.wang,fxp}@dlmu.edu.cn, pengjinjia@hbu.edu.cn,

ruoxii.deng@gmail.com, yangwang@hfut.edu.cn

Abstract

Unsupervised person search aims to localize a particular target person from a gallery set of scene images without annotations, which is extremely challenging due to the unexpected variations of the unlabeled domains. However, most existing methods dedicate to developing multi-stage models to adapt domain variations while using clustering for iterative model training, which inevitably increases model complexity. To address this issue, we propose a Fast One-stage Unsupervised person Search (FOUS) which complementary integrates domain adaptation with label adaptation within an end-to-end manner without iterative clustering. To minimize the domain discrepancy, FOUS introduced an Attention-based Domain Alignment Module (ADAM) which can not only align various domains for both detection and ReID tasks but also construct an attention mechanism to reduce the adverse impacts of low-quality candidates resulting from unsupervised detection. Moreover, to avoid the redundant iterative clustering mode, FOUS adopts a prototype-guided labeling method which minimizes redundant correlation computations for partial samples and assigns noisy coarse label groups efficiently. The coarse label groups will be continuously refined via label-flexible training network with an adaptive selection strategy. With the adapted domains and labels, FOUS can achieve the state-of-the-art (SOTA) performance on two benchmark datasets, CUHK-SYSU and PRW. The code is available at <https://github.com/whbdmu/FOUS>

1 Introduction

The objective of the pedestrian search task is to identify and locate specific individuals within panoramic images. Initially, all pedestrians present in the image are detected, and subsequently, they are compared to the target pedestrian image for recognition. In the context of the intelligent security field, it becomes increasingly difficult and costly to complete person

*Corresponding author

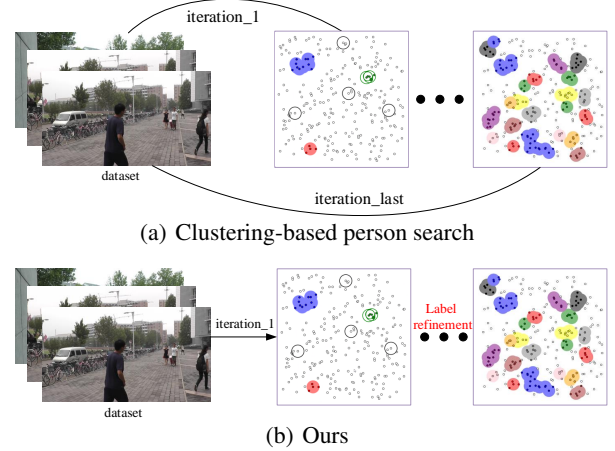


Figure 1: Differences in operation between our proposed method and mainstream methods. (a) represents that the clustering algorithm utilizes the original data to calculate similarity in each iteration. (b) illustrates that our proposed method utilizes the original data only in the first iteration to assign soft labels, and then gradually refines the labels.

search tasks in a supervised manner due to the massive volume of videos and pictures generated by numerous cameras. Therefore, unsupervised domain adaptive methods should receive more attention.

The main challenges currently in unsupervised pedestrian search are the lack of bounding box annotations and the lack of pedestrian identity label annotations. Since it is very difficult to directly train unsupervised detection and re-identification, a series of weakly supervised research works [Yan *et al.*, 2022; Han *et al.*, 2021; Jia *et al.*, 2023] have been proposed to address the challenge of lacking identity annotations, which have employed clustering techniques to assign pseudo labels. As shown in Fig.1(a), clustering approaches typically require multiple iterations of calculating sample similarity, which can be time-consuming and resource-intensive. Moreover, these methods still demand significant time and effort to annotate ground-truth bounding boxes, and their model generalization capability is limited, rendering them unsuitable for real-world scenarios.

Therefore, unsupervised person search was emerged as the times require. Considering the difficulty and impracticality of

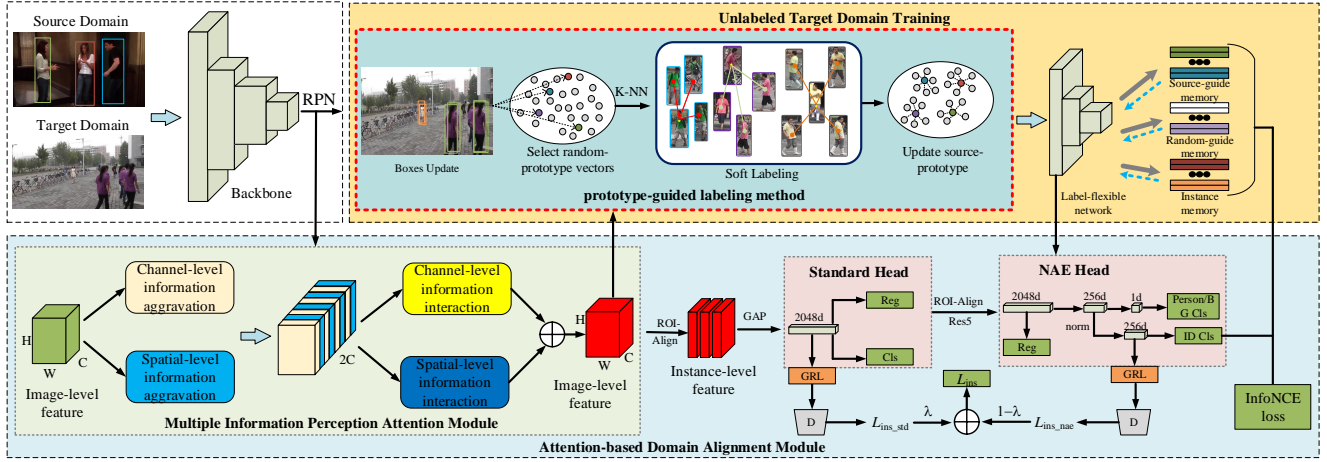


Figure 2: The design architecture of the FOUS framework. For each iteration, after extracting features, FOUS alternates between two phases: (1) Attention-based Domain Alignment.(Sec. 2.2) The candidate box quality is enhanced through the Multi-Information Perception Attention Module, followed by domain alignment operations. (2) Unlabeled Target Domain Training.(Sec. 2.3) Annotate the unlabeled samples in the target domain utilizing prototypes as the reference for further fine-tuning, in which select random features as the target prototype vectors and update the learned source prototypes.

directly training unsupervised detection and re-identification, current research methods rely on powerful pre-trained models. Li et al.[4] introduced a domain adaptive method to address the challenge of unsupervised pedestrian search by training on a labeled dataset from the source domain. Specifically, Li et al. designed a domain alignment module to alleviate the difference between unsupervised detection and re-identification subtasks, and then proposed a dynamic clustering strategy to generate pseudo labels on the target domain. We can observe that the clustering method, which is widely employed in both weakly supervised and unsupervised person re-identification tasks, offers certain advantages. It is capable of withstanding noisy labels and generating dependable labels, thus effectively training a model with robust generalization capabilities. However, the computational resources required for this method are quite demanding. The clustering method involves calculating pairwise similarities and multiple iterations to optimize results, which can result in an impractical computational burden. Consequently, these methods face challenges when applied to smart security scenarios involving a massive amount of video footage.

In order to solve this problem, this paper proposes a fast and efficient unsupervised domain adaptation framework for the person search task, which can learn a model with strong generalization ability at a lower cost. As illustrated in Fig.1(b), different from the clustering methods of existing models, FOUS gives up generating relatively accurate labels through complex clustering algorithms, and instead tries to learn potential correlations from soft labels with greater noise and fewer resources. First, in order to quickly assign soft labels, we use the prototype correlation labeling method to calculate the similarity between partial samples only once. To reduce computational resources, these prototypes are used as annotators to soft-label unlabeled samples based on nearest neighbor correlations. Secondly, considering the importance

of mitigating the impact of generated noisy labels, we follow the domain alignment module in DAPS and introduce a new attention mechanism, which can amplify global-dimensional interaction features while reducing information dispersion. Effectively reduce the number of noisy labels generated by low-quality candidate frames in unsupervised detection. And FOUS also proposes an adaptive selection strategy to perform label-flexible training of the network to gradually refine the rough labels.

Our contributions can be summarized as follows:

1. We introduce a fast unsupervised domain-adaptive pedestrian search framework based on a prototype correlation labeling method instead of the prevalent clustering algorithm. Compared with multiple iterations of the clustering algorithm, FOUS only calculates the similarity between some samples once and directly assigns soft label groups.
2. In order to reduce the noise in the soft label group, we first introduce a new attention mechanism to alleviate the differences between unsupervised detection and re-identification tasks, and also propose an adaptive selection strategy to gradually refine the coarse labels to find reliable and similar target images.
3. Without any auxiliary labels in the target domain, our method achieves good performance on both pedestrian search benchmark datasets, which not only reduces the amount of calculation and improves the inference speed but also has good generalization ability.

2 Method

2.1 Framework Overview

Fig.2 highlights the design architecture of the proposed FOUS framework. Given the input images from both the source and the target domain, we utilize a pre-trained model on the source domain annotation dataset to produce the source-prototype vector, and the image-level feature maps

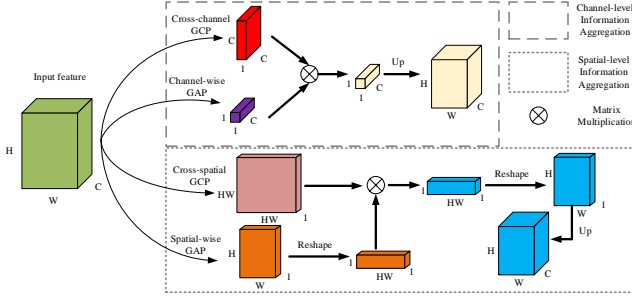


Figure 3: The channel-level information aggregation and spatial-level information aggregation in ADAM.

are extracted with a backbone network. Next, these features are fed into the Region Proposal Network (RPN) to generate proposals, which are passed through the attention module to create instance-level feature maps. To bridge the domain gaps and ensure effective detection and ReID (Re-Identification) tasks, we introduce an attention-based domain alignment module (ADAM). The ADAM is designed to align both image-level and instance-level features across different domains. It helps harmonize the representations and close the gap between domains.

To tackle the issue of computational cost in unsupervised reID tasks, a new prototype-guided labeling method is proposed to assign and optimize soft labels instead of computationally complex clustering methods, which frees up the process of label generation, including prototypes-guided labeling phase and label-flexible training phase. We first annotate the unlabeled samples with coarse labels in a simple way, which selects the prototype vectors generated above and softly annotates unlabeled samples via the relevance between these prototypes and samples. Additionally, FOUS trains its models using a combination of cluster-level contrastive loss and instance-level loss, which ensures that the models adhere to both the constraints imposed by the two types of losses. It aims to refine the coarse labels by incorporating the proposed adaptive selection strategy. Above all, except for the initial iteration, the labeled samples from the source domain are not utilized in our FOUS.

2.2 Attention-based Domain Alignment Module

Attention Mechanism. To mitigate the negative effects of low-quality proposals that arise from unsupervised detection, a novel attention module is designed, which can amplify global-dimensional interactive features while reducing information dispersion. Fig.2 emphasizes that the attention module primarily consists of information aggregation and information interaction.

Input feature $x \in \mathbb{R}^{H \times W \times C}$ is initially processed into feature $x^c \in \mathbb{R}^{H \times W \times C}$ and feature $x^s \in \mathbb{R}^{H \times W \times C}$ through channel-level information aggregation and spatial-level information aggregation respectively. And these two features are subsequently cross-connected in the channel dimension to yield features $x^{cs} \in \mathbb{R}^{H \times W \times 2C}$. The information aggregation is formulated as:

$$x^{cs} = \text{Concat}(f_{clia}(x), f_{slia}(x)), \quad (1)$$

where f_{clia} , f_{slia} and Concat represent channel-level information aggregation, spatial-level information aggregation and cross-connection, respectively. Channel-level information aggregation can capture channel dependency information, channel structure information, and spatial global information through cross-channel global covariance pooling and channel-level global average pooling. Spatial-level information aggregation can capture spatial dependency information, spatial structure information, and channel global information through cross-spatial global covariance pooling and spatial-level global average pooling. Cross-connection plays an important role in organizing various pieces of information, enabling effective interaction and integration of subsequent information.

Fig.3 illustrates the specific structure of channel-level information aggregation and spatial-level information aggregation in ADAM, which can simultaneously achieve the perception of multi-dimensional dependency information, multi-dimensional global information and multi-dimensional structural information in information aggregation. The channel-level information aggregation is formulated as follows:

$$f_{clia}(x) = \text{Up}(MM(CcGCP(x), CwGAP(x))) \quad (2)$$

where $CcGCP$, $CwGAP$, MM and Up represent cross-channel global covariance pooling, channel-wise global average pooling, matrix multiplication and upsampling operations, respectively. Moreover, the spatial-level information aggregation is formulated as follows:

$$f_{slia}(x) = \text{Up}\left(MM\left(SwGAP(x)^\Delta, CsGCP(x)^\Delta\right)\right) \quad (3)$$

where $SwGAP$, $CsGCP$ and Δ represent spatial-wise global average pooling, cross-spatial global covariance pooling and reshape operations, respectively.

Similarly, feature $x^{cs} \in \mathbb{R}^{H \times W \times 2C}$ is separated into feature $x^{c's} \in \mathbb{R}^{H \times W \times C}$ and feature $x^{s'c} \in \mathbb{R}^{H \times W \times C}$ through channel-driven information interaction and spatial-driven information interaction respectively. And these two features are subsequently adaptively fused into features $x^{c's'} \in \mathbb{R}^{H \times W \times C}$ by allocating learnable parameters $\alpha \in \mathbb{R}^{1 \times 1 \times C}$ and $\beta \in \mathbb{R}^{1 \times 1 \times C}$. The information interaction is formulated as:

$$x^{c's'} = \alpha f_{cdii}(x^{cs}) + \beta f_{sdi}(x^{cs}), \quad (4)$$

where f_{cdii} and f_{sdi} represent channel-driven information interaction and space-driven information interaction, respectively. Channel-driven interaction focuses on perceiving diversity in channels by assigning unique parameters along the channel dimension while sharing the same parameters in the spatial dimension. On the other hand, spatial-driven interaction aims to perceive diversity in space by assigning distinct parameters along the spatial dimension while sharing the same parameters in the channel dimension.

Fig.4 shows the specific structure of channel-level information interaction and spatial-level information interaction in ADAM, which concurrently achieves the perception of multidimensional diverse information during information interaction. ADAM stimulates intrinsic information potential through a more comprehensive proactive interaction. The

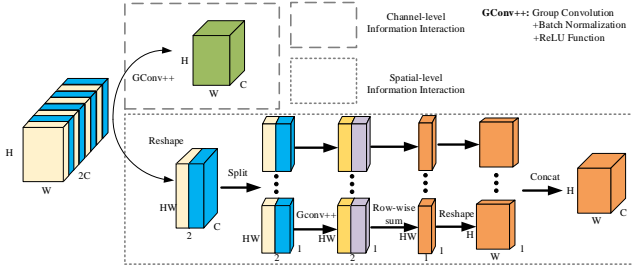


Figure 4: The channel-level information interaction and spatial-level information interaction in ADAM.

channel-level information interaction is formulated as follows:

$$f_{cdii}(x^{cs}) = GConv_{++}(x^{cs}) \quad (5)$$

where $GConv$ represents the combination of group convolution, batch normalization, and the ReLU function. The information interaction between different groups is undisturbed. Channel-driven information interaction, achieved by assigning different parameters in the channel dimension and sharing the same information parameters in the spatial dimension, not only facilitates the interaction and fusion of multiple information in channel-level and spatial-level information collection but also further perceives channel diversity information.

The spatial-level information interaction is formulated as follows:

$$f_{sdi}(x^{cs}) = Concat \left(Sum(GConv_{++}(Split(x^{cs\Delta})))^\Delta \right) \quad (6)$$

where Sum represents the row-wise summation. Reshaping and splitting operations are used to adjust the feature shape for subsequent specific information interactions. The spatial-driven information interaction, achieved by assigning different parameters in the spatial dimension and sharing the same parameters in the channel dimension, not only facilitates the interaction and fusion of multiple information from channel-level and spatial-level information collection but also further perceives spatial diversity information.

Finally, feature $x^{c's'} \in \mathbb{R}^{H \times W \times C}$ is activated into the attention map by the sigmoid function. The attention map is employed to modulate input sub-feature $x \in \mathbb{R}^{H \times W \times C}$, resulting in the output sub-feature $x' \in \mathbb{R}^{H \times W \times C}$:

$$x' = x Sigmoid(x^{c's'}) \quad (7)$$

The sigmoid function distinguishes the importance by activating eigenvalues within the range of 0 to 1. Importantly, the input sub-features are transformed into output sub-features across all branches. This multi-branch structure is advantageous in activating different attention mechanisms, allowing for the selective perception of valuable feature information on each branch in a targeted manner.

Task-sensitive Domain Alignment. As studied by [Chen *et al.*, 2018b; You *et al.*, 2019; Xu *et al.*, 2020; Wang *et al.*, 2024], reducing domain disparities is advantageous for both subtasks within person search, and can enhance the model’s capacity to learn domain-invariant representations. Given

the swift advancement of domain-adaptive detectors [Khodabandeh *et al.*, 2019; Wang, 2021; Vibashan *et al.*, 2023; Zhang *et al.*, 2023], FOUS proposes a task-sensitive domain alignment module. As shown in Fig.2, ADAM uses a patch-based domain classifier to predict the domain from which the input features come, and uses a minmax formula to mislead the domain classifier and encourage domain-invariant representation learning. Assuming we possess N training images $\{I_1, \dots, I_N\}$ along with their respective domain labels, where 0 and 1 represent the source domain and target domain respectively. Then denote the domain classifier as D , and further denote the domain prediction result of the input feature I_i as p_i . We incorporate a cross-entropy loss for domain alignment through an adversarial training approach:

$$L_{dom} = - \sum_i [d_i \log p_i + (1 - d_i) \log(1 - p_i)] \quad (8)$$

Based on the characteristics of the upstream and downstream tasks, we suggest achieving balance in the task-sensitive alignment module by equitably adjusting the alignment weights of instance-level features in both sub-tasks. The instance-level loss can be formulated as:

$$L_{ins} = - \lambda \sum_{i,j} [d_i \log p_{i,j}^d + (1 - d_i) \log(1 - p_{i,j}^d)] - (1 - \lambda) \sum_{i,k} [d_i \log p_{i,k}^r + (1 - d_i) \log(1 - p_{i,k}^r)] \quad (9)$$

where $j \in \{1, \dots, K_1\}$ and $k \in \{1, \dots, K_2\}$. The source domain comprises N_s images, while the target domain includes N_t images. The balancing factor λ is set as:

$$\lambda = \sigma \left(4 \cdot \text{sign}(N_t - N_s) \left(\frac{\max(N_s, N_t)}{\min(N_s, N_t)} - 1 \right) \right) \quad (10)$$

where σ is Sigmoid function employed for domain normalization. What’s more, we introduce an L2-norm regularizer to maintain consistency between image-level and instance-level classifiers.

2.3 Unlabeled Target Domain Training

FOUS employs a prototype-relevance labeling method as a replacement for complex clustering algorithms, leading to a significant reduction in computational costs. In FOUS, the prototype vector needs to be initially selected or calculated, followed by the computation of the correlation between the prototype vector and all the samples. Then assign the label of the nearest prototype vector to the sample as a pseudo label. Therefore, the selection of the prototype vector is a critical aspect. And FOUS design two types of prototypes, namely the source-prototype vector and the random-prototype vector. Initially, the source-prototype vector is computed using well-labeled data from the source domain. Subsequently, to enhance FOUS’s adaptability in the target domain, features are randomly selected from the target domain to create a random-prototype vector.

Prototype vector initialization We utilize the network $E_s(\cdot)$, pre-trained on the source domain, to extract features from the source domain samples. Subsequently, based on the

ground-truth labels, the source-prototype vector can be computed as:

$$P_k^s = \frac{1}{N_k} \sum_{f_i \in F_k^s} f_i \quad (11)$$

where F_k^s represents a set of features with the same labels k . f_i is the feature of each instance. N_k is the number of samples with the label k . The source-prototype vector P^s is composed of $\{P_1^s, \dots, P_K^s\}$, $k \in [1, K]$. Particularly, K means the number of identity categories in the source domain. However, models trained solely on pseudo-labels generated from source-prototype vectors tend to be sensitive to variations in the target domain and are susceptible to introducing a considerable amount of noise. Hence, FOUS sets up random prototype vectors in the target domain to enhance diversity. Similar to the source-prototype, $E_s(\cdot)$ is employed to extract features from target domain samples. Subsequently, N_t vectors are randomly selected to form the random-prototype $P^t = \{P_1^t, \dots, P_{N_t}^t\}$.

Labeling Once the source and random prototype vector are calculated, the labels for other sample instances in the target domain are determined by the k-Nearest Neighbor algorithm,

$$l_i^s = \arg \min_{l_s} \text{dist}(f_i, P^s) \quad (12)$$

where $\text{dist}(a, b)$ means the Euclidean distance between a and b . f_i is the characteristic of the i -th instance. Eq.12 signifies assigning the instance with the label of the vector in P^s that is closest to f_i . All the labeled images collectively constitute a new dataset D^s . Similar to D^s , according to the random-prototype P^t , we can also derive a group of labels,

$$l_i^t = \arg \min_{l_t} \text{dist}(f_i, P^t) \quad (13)$$

The assignment of pseudo labels through prototypes results in the creation of two datasets, which are $D^s = \{(x_i, l_1^s, \dots, l_n^s)\}_{i=1}^N$ and $D^t = \{(x_i, l_1^t, \dots, l_n^t)\}_{i=1}^N$, n represents the number of instances in x_i . Then, the source-prototype is updated by the target datasets with pseudo labels,

$$P_j^s = \frac{1}{N_j} \sum_{f \in F_j^t} f \quad (14)$$

where F_j^t means the features belonging to the cluster j . Therefore, FOUS does not use images from the source domain except for the first iteration.

Label-flexible Training To improve the training of models with flexible labels, FOUS constructs distinct memory structures to store features based on different label groups. Based on the source prototype P^s and random prototype P^t , the pseudo labels L^s and L^t can be calculated. To mitigate the influence of noise, we designed two cluster-level memory structures to store the features at the training stage. Taking the L^s as an example, the features $\{c_1, \dots, c_K\}$ of each cluster are stored in a memory-based feature dictionary. K means the number of clusters. After clustering with prototypes, the features in the cluster are utilized to initialize the memory dictionary, which could be expressed as,

$$m_k = \frac{1}{N_k} \sum_{f \in F_k} f \quad (15)$$

where F_k represents the feature set of instances labeled as k , comprising all feature vectors in cluster k . N_k is the number of features in F_k . When employing random-guided memory, we are provided with a query instance q and perform feature comparisons with all features within the respective memory $\{m_1^t, \dots, m_K^t\}$ structure utilizing the InfoNCE loss,

$$L_c^t = -\log \frac{\exp(\text{sim}(f \cdot m_+^t)/\tau)}{\sum_{k=1}^K \exp(\text{sim}(f \cdot m_k^t)/\tau)} \quad (16)$$

where m_+^t denotes the features that share the same identity as f within the random-guided memory. τ is the proportional coefficient balancing factor. Similar to Eq.16, the loss L_c^s of the source-guided memory also could be calculated.

In addition, FOUS employs invariant learning between images to bolster the model's generalization capability. An instance-level memory bank $\{m_1^l, \dots, m_N^l\}$ is consequently established to store all features, and soft labels are estimated by evaluating the correlation between images.

Due to the absence of genuine labels, neighborhoods displaying high correlation play a role in diminishing the distance between similar images. Consequently, FOUS introduces an adaptive selection strategy. Taking inspiration from [Ding *et al.*, 2020; Peng *et al.*, 2020; Wang *et al.*, 2022], a similarity threshold is defined. Only when the distance between the adaptively chosen neighbors and the provided image falls below this threshold, these samples are presumed to share the same label as the target image. Therefore, these samples should exhibit closer proximity to the target image. The corresponding loss can be formulated as:

$$L_t^e = -\frac{1}{N} \sum_{j=1}^N \sum_{i=1, j \neq i}^N v_j^i \log p(i|m_j^t) \quad (17)$$

where $v_j \in \{0, 1\}^N$. If $v_j^i = 1$, it means the i -th image is a reliable neighborhood of the j -th image. If $v_j^i = 0$, the i -th image is abandoned.

Final loss The final loss is composed of detection loss and re-id loss, which is formulated as,

$$L = L_{ins} + L_c^t + L_c^s + L_t^e + L_s^e \quad (18)$$

where L_{ins} is calculated by Eq.9. L_c^t and L_c^s are calculated by Eq.16. L_t^e and L_s^e are calculated by Eq.17.

3 Experiments

3.1 Datasets and Evaluation metrics

Datasets The proposed method is evaluated on two large-scale benchmark datasets, CUHK-SYSU[Xiao *et al.*, 2017] and PRW[Zheng *et al.*, 2017]. CUHK-SYSU consists of 12,490 images captured by real surveillance cameras and 5,694 images from movies and TV shows. The training set comprises 11,206 images and 5,532 query persons, while the test set includes 6,978 images and 2,900 query persons. The widely utilized PRW dataset comprises a total of 11,816 video frames captured by 6 cameras and 2,057 queries with 932 identities.

Evaluation metrics In the dataset configuration, annotations for the source domain dataset are available, while the

Table 1: Comparison of mAP(%) and rank-1 accuracy(%) with the state-of-the-art on CUHK-SYSU and PRW

Method		CUHK-SYSU		PRW		
		mAP	top-1	mAP	top-1	
two-stage	DPM [Girshick <i>et al.</i> , 2015]	-	-	20.5	48.3	
	MGTS [Chen <i>et al.</i> , 2018a]	83.0	83.7	32.6	72.1	
	CLSA [Lan <i>et al.</i> , 2018]	87.2	88.5	38.7	65.0	
	IGPN [Dong <i>et al.</i> , 2020]	90.3	91.4	47.2	87.0	
	RDLR [Han <i>et al.</i> , 2019]	93.0	94.2	42.9	70.2	
	TCTS [Wang <i>et al.</i> , 2020a]	93.9	95.1	46.8	87.5	
end-to-end	OIM [Xiao <i>et al.</i> , 2017]	75.5	78.7	21.3	49.4	
	IAN [Xiao <i>et al.</i> , 2019]	76.3	80.1	23.0	61.9	
	NPSM [Liu <i>et al.</i> , 2017]	77.9	81.2	24.2	53.1	
	RCAA [Chang <i>et al.</i> , 2018]	79.3	81.3	-	-	
	CTXG [Yan <i>et al.</i> , 2019]	84.1	86.5	33.4	73.6	
	QEEPS [Munjal <i>et al.</i> , 2019]	88.9	89.1	37.1	76.7	
	APNet [Zhong <i>et al.</i> , 2020]	88.9	89.3	41.9	81.4	
	HOIM [Chen <i>et al.</i> , 2020a]	89.7	90.8	39.8	80.4	
	NAE [Chen <i>et al.</i> , 2020b]	91.5	92.4	43.3	80.9	
	NAE+ [Chen <i>et al.</i> , 2020b]	92.1	92.9	44.0	81.1	
	AlignPS [Yan <i>et al.</i> , 2021]	94.0	94.5	46.1	82.1	
	SeqNet [Li and Miao, 2021]	93.8	94.6	46.7	83.4	
	Ours	FOUS	78.7	80.5	35.4	80.8

ground truth boxes and identity information for the target domain dataset are not accessible. We employ widely used metrics such as mean average precision(mAP) and cumulative matching characteristic(CMC) top-1 accuracy for evaluating the re-identification subtask. For the detection task, average precision(AP) and recall rate are adopted as the evaluation metrics.

3.2 Implementation Details

Our experiments are implemented on NVIDIA GeForce GTX 3090Ti GPU with Pytorch[Paszke *et al.*, 2017]. FOUS utilize ResNet50[He *et al.*, 2016] pre-trained on ImageNet-1k[Deng *et al.*, 2009] as the default backbone network. During the training process, the dimensions of input images are adjusted to 1500×900 , and random horizontal flipping is applied for data augmentation. We employ the Stochastic Gradient Descent(SGD) method to optimize the model, with a mini-batch size set to 4 and a learning rate of 0.003. The momentum and weight decay are set to 0.9 and 5×10^{-4} , respectively. For the k-nearest neighbor algorithm, the number of neighbors is set to 1. When PRW is chosen as the target domain, we pre-train on the source domain CUHK-SYSU for 8 epochs and subsequently engage in joint training for 10 epochs. Similarly, when CUHK-SYSU is chosen as the target domain, we pre-train on the source domain PRW for 2 epochs and subsequently engage in joint training for 14 epochs. However, the similarity between source domain samples is computed only once.

3.3 Comparison with State-of-the-Art Methods

As there is currently limited interest in unsupervised pedestrian search methods, we begin by comparing FOUS with fully supervised methods in Table.1, encompassing both two-stage and end-to-end methods. For the first time, we eliminate the need for computationally expensive clustering algorithms in assigning labels for weakly supervised and unsupervised pedestrian search tasks. Surprisingly, FOUS outper-

Table 2: Comparison of mAP(%) and rank-1 accuracy(%) with the weakly supervised and unsupervised methods on CUHK-SYSU and PRW

Methods	CUHK-SYSU		PRW	
	map	top-1	map	top-1
<i>weakly supervised:</i>				
CGPS[Yan <i>et al.</i> , 2022]	80.0	82.3	16.2	68.0
R-SiamNet[Han <i>et al.</i> , 2021]	86.0	87.1	21.2	73.4
DICL[Jia <i>et al.</i> , 2023]	87.4	88.8	35.5	80.9
SSL[Wang <i>et al.</i> , 2023]	87.4	88.5	30.7	80.6
<i>unsupervised:</i>				
DAPS[Li <i>et al.</i> , 2022]	77.6	79.6	34.7	80.6
Ours	78.7	80.4	35.4	80.8

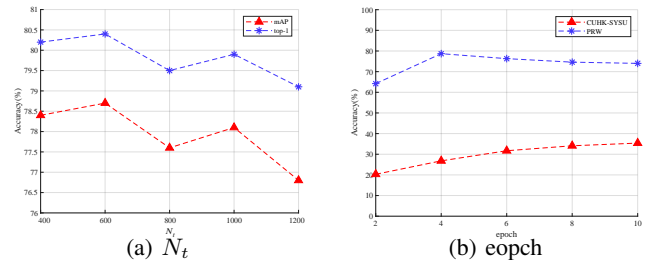


Figure 5: (a) represents the influence of varying the number of random prototypes on the map and top-1 metrics on the CUHK-SYSU dataset. (b) illustrates the impact of different pre-training rounds on two datasets.

forms some supervised methods. The experimental results indicate a substantial gap between FOUS and state-of-the-art supervised methods. We aspire that our approach may serve as a catalyst for subsequent explorations in this field.

We present a comparison of FOUS with state-of-the-art weakly supervised and unsupervised methods in Table.2. Surprisingly, FOUS exhibits superior performance on the PRW dataset compared to all weakly supervised and unsupervised methods. For the CUHK-SYSU dataset, FOUS surpasses the existing unsupervised method DAPS by 1% in mAP and 1.2% in top-1, although it has not yet reached the level of performance achieved by weakly supervised methods. The reason may be as mentioned in DAPS. Since the number of images and identities in PRW is significantly less than in CUHK-SYSU, the detection performance of CUHK-SYSU as the target domain is poor, further leading to lower accuracy in the search task. The proposed attention-based domain alignment module enhances the quality of proposals, further bolstering the performance of detection in FOUS. Consequently, FOUS achieves a balance between reducing computational complexity, accelerating processing speed, and maintaining stable accuracy.

3.4 Ablation Study

In this subsection, we perform ablation experiments to validate the significance of each component in FOUS. In Table.3, we compare the combination of baseline methods with different proposed modules and report the results on both CUHK-SYSU and PRW datasets. The baseline model achieves 50.4% mAP and 52.8% Top-1 accuracy on the CUHK-SYSU

Table 3: Validating the effectiveness of different modules on CUHK and PRW datasets. AM: Attention Mechanism. TDA: Task-sensitive Domain Alignment. LFT: Label-flexible Training

AM	TDA	LFT	CUHK-SYSU		PRW	
			map	top-1	map	top-1
			50.4	52.8	26.7	74.6
✓	✓		68.1	71.6	33.2	80.4
	✓	✓	64.3	66.9	28.0	77.1
✓		✓	72.3	75.7	32.9	80.2
✓	✓	✓	78.7	80.4	35.4	80.8

dataset. FOUS implemented three components and achieved a 28.2% mAP and 28.0% top-1 improvement over the baseline. We find that if only use the prototype-guided labeling method to generate coarse label groups without utilizing the label-flexible network to refine the labels, the accuracy will decrease significantly by 10% on CUHK-SYSU and 7% on PRW. If the attention mechanism is abandoned to enhance proposals, the accuracy drops even further to 14.3% on CUHK-SYSU. Furthermore, neglecting the domain difference between the two subtasks leads to a reduction in accuracy by 6.3% on CUHK. Hence, the three components we proposed effectively enhance the performance and generalization ability of the model.

Furthermore, to verify the effectiveness of the designed attention module, we compared it with state-of-the-art attention methods. As shown in Table.5, our proposed attention module outperforms significantly, achieving an average accuracy 1.8 higher than CBAM, ECAM, SGEM, and GCT methods on CUHK-SYSU. We can confidently infer that global information aggregation and interaction with proposals are beneficial for model learning.

Last but not least, we compare with state-of-the-art weakly supervised and unsupervised methods in terms of network parameter amount and computational effort. Table.4 presents the comparative results concerning computational requirements, parameter count, training time per iteration, and accuracy during the process. As FOUS computes the similarity of source domain samples only once, it reduces computational costs by nearly half compared to DAPS, which utilizes clustering algorithms. This reduction is achieved at a minor cost in terms of parameters. Furthermore, training time is relatively reduced by 25%, and there is a remarkable improvement in accuracy rather than a decline. We have abandoned the complex clustering method and, instead, proposed a prototype correlation labeling algorithm, resulting in a significant reduction in the number of parameters and computational workload.

3.5 Parameter analysis

Setting several parameters in FOUS may affect the performance of the model. Therefore, we evaluate these parameters in our paper, such as the number of random-prototype vectors and the pre-trained epochs during the training stage. The results on CUHK-SYSU and PRW under different settings are shown in Fig.5.

Analysis of the random selected prototype number As shown in Fig.5(a), we vary the number of random prototype

Table 4: Comparing the network parameters and computational requirements with weakly supervised and unsupervised methods on PRW.

Methods	GFLOPS	PRARMS	Time	map	top-1
CGPS	281	49.2M	1.1h	16.2	68.0
R-SiamNet	320	52.5M	1h	21.4	75.2
DAPS	628	53.4M	1.6h	34.7	80.6
Ours	388	53.6M	1.2h	35.4	80.8

Table 5: Validating the effectiveness of different attention mechanism on CUHK and PRW datasets.

Attention Models	CUHK-SYSU		PRW	
	map	top-1	map	top-1
CBAM[Woo <i>et al.</i> , 2018]	77.2	79.0	33.6	79.4
ECAM[Wang <i>et al.</i> , 2020b]	76.2	78.1	30.1	78.6
SGEM[Li <i>et al.</i> , 2019]	77.0	78.7	32.3	80.1
GCT[Ruan <i>et al.</i> , 2021]	76.8	77.9	32.6	80.2
Ours	78.7	80.4	35.4	80.8

vectors N_t to 400, 600, 800, 1000, and 1200 on CUHK-SYSU, respectively. And N_t is set to 100, 200, 300, 400, 500 on PRW, respectively. In detail, maintaining the parameters of batch size and pretraining rounds unchanged, as illustrated in Figure 3, the model performance varies with the different settings of N_t . This underscores the significance of randomly selecting the number of prototypes for generating pseudo-labels. What’s more, Fig.5(a) also shows that $N_t = 600$ and $N_t = 300$ can achieve the best accuracy on CUHK-SYSU and PRW, respectively.

Analysis of the pre-trained epochs In this part, the paper explores the relations between the pre-trained epochs and the whole model performance. As observed in Fig.5(b), when CUHK-SYSU is embraced as the target domain, the performance peaks at a pre-trained epoch of 10, while with epoch = 4 for PRW. Our analysis of this result is that in smaller source domains, even limited additional target information may contribute to cross-domain generalization. In contrast, for larger source datasets, unreliable target suggestions may have a negative impact on mitigating domain differences.

4 Conclusion

In this paper, we present the FOUS framework designed for the domain adaptive pedestrian search task. FOUS introduces two components, one is a prototype-guided labeling algorithm, which replaces the commonly used complex clustering algorithms in this domain, significantly reducing computational costs at the expense of accuracy. The other is an attention-based domain alignment module, alleviating the impact of low-quality candidate boxes on re-identification tasks in unsupervised detection. Together, these components complement each other, reducing computational overhead while enhancing the model’s performance. Judging from the results, experiments on two foundational datasets demonstrate the performance of FOUS and the effectiveness of the introduced modules and achieve state-of-the-art performance.

References

- [Chang *et al.*, 2018] Xiaojun Chang, Po-Yao Huang, Yi-Dong Shen, Xiaodan Liang, Yi Yang, and Alexander G Hauptmann. Rcaa: Relational context-aware agents for person search. In *Proceedings of the European Conference on Computer Vision (ECCV)*, pages 84–100, 2018.
- [Chen *et al.*, 2018a] Di Chen, Shanshan Zhang, Wanli Ouyang, Jian Yang, and Ying Tai. Person search via a mask-guided two-stream cnn model. In *Proceedings of the european conference on computer vision (ECCV)*, pages 734–750, 2018.
- [Chen *et al.*, 2018b] Yuhua Chen, Wen Li, Christos Sakaridis, Dengxin Dai, and Luc Van Gool. Domain adaptive faster r-cnn for object detection in the wild. In *Proceedings of the IEEE conference on computer vision and pattern recognition*, pages 3339–3348, 2018.
- [Chen *et al.*, 2020a] Di Chen, Shanshan Zhang, Wanli Ouyang, Jian Yang, and Bernt Schiele. Hierarchical online instance matching for person search. In *Proceedings of the AAAI Conference on Artificial Intelligence*, volume 34, pages 10518–10525, 2020.
- [Chen *et al.*, 2020b] Di Chen, Shanshan Zhang, Jian Yang, and Bernt Schiele. Norm-aware embedding for efficient person search. In *Proceedings of the IEEE/CVF conference on computer vision and pattern recognition*, pages 12615–12624, 2020.
- [Deng *et al.*, 2009] Jia Deng, Wei Dong, Richard Socher, Li-Jia Li, Kai Li, and Li Fei-Fei. Imagenet: A large-scale hierarchical image database. In *2009 IEEE conference on computer vision and pattern recognition*, pages 248–255. Ieee, 2009.
- [Ding *et al.*, 2020] Yuhang Ding, Hehe Fan, Mingliang Xu, and Yi Yang. Adaptive exploration for unsupervised person re-identification. *ACM Transactions on Multimedia Computing, Communications, and Applications (TOMM)*, 16(1):1–19, 2020.
- [Dong *et al.*, 2020] Wenkai Dong, Zhaoxiang Zhang, Chunfeng Song, and Tieniu Tan. Instance guided proposal network for person search. In *Proceedings of the IEEE/CVF Conference on Computer Vision and Pattern Recognition*, pages 2585–2594, 2020.
- [Girshick *et al.*, 2015] Ross Girshick, Forrest Iandola, Trevor Darrell, and Jitendra Malik. Deformable part models are convolutional neural networks. In *Proceedings of the IEEE conference on Computer Vision and Pattern Recognition*, pages 437–446, 2015.
- [Han *et al.*, 2019] Chuchu Han, Jiacheng Ye, Yunshan Zhong, Xin Tan, Chi Zhang, Changxin Gao, and Nong Sang. Re-id driven localization refinement for person search. In *Proceedings of the IEEE/CVF International Conference on Computer Vision*, pages 9814–9823, 2019.
- [Han *et al.*, 2021] Chuchu Han, Kai Su, Dongdong Yu, Zehuan Yuan, Changxin Gao, Nong Sang, Yi Yang, and Changhu Wang. Weakly supervised person search with region siamese networks. In *Proceedings of the IEEE/CVF International Conference on Computer Vision*, pages 12006–12015, 2021.
- [He *et al.*, 2016] Kaiming He, Xiangyu Zhang, Shaoqing Ren, and Jian Sun. Deep residual learning for image recognition. In *Proceedings of the IEEE conference on computer vision and pattern recognition*, pages 770–778, 2016.
- [Jia *et al.*, 2023] Chengyou Jia, Minnan Luo, Caixia Yan, Linchao Zhu, Xiaojun Chang, and Qinghua Zheng. Collaborative contrastive refining for weakly supervised person search. *IEEE Transactions on Image Processing*, 2023.
- [Khodabandeh *et al.*, 2019] Mehran Khodabandeh, Arash Vahdat, Mani Ranjbar, and William G Macready. A robust learning approach to domain adaptive object detection. In *Proceedings of the IEEE/CVF International Conference on Computer Vision*, pages 480–490, 2019.
- [Lan *et al.*, 2018] Xu Lan, Xiatian Zhu, and Shaogang Gong. Person search by multi-scale matching. In *Proceedings of the European conference on computer vision (ECCV)*, pages 536–552, 2018.
- [Li and Miao, 2021] Zhengjia Li and Duoqian Miao. Sequential end-to-end network for efficient person search. In *Proceedings of the AAAI Conference on Artificial Intelligence*, volume 35, pages 2011–2019, 2021.
- [Li *et al.*, 2019] Xiang Li, Xiaolin Hu, and Jian Yang. Spatial group-wise enhance: Improving semantic feature learning in convolutional networks. *arXiv preprint arXiv:1905.09646*, 2019.
- [Li *et al.*, 2022] Junjie Li, Yichao Yan, Guanshuo Wang, Fufu Yu, Qiong Jia, and Shouhong Ding. Domain adaptive person search. In *European Conference on Computer Vision*, pages 302–318. Springer, 2022.
- [Liu *et al.*, 2017] Hao Liu, Jiashi Feng, Zequn Jie, Karlekar Jayashree, Bo Zhao, Meibin Qi, Jianguo Jiang, and Shuicheng Yan. Neural person search machines. In *Proceedings of the IEEE International Conference on Computer Vision*, pages 493–501, 2017.
- [Munjal *et al.*, 2019] Bharti Munjal, Sikandar Amin, Federico Tombari, and Fabio Galasso. Query-guided end-to-end person search. In *Proceedings of the IEEE/CVF Conference on Computer Vision and Pattern Recognition*, pages 811–820, 2019.
- [Paszke *et al.*, 2017] Adam Paszke, Sam Gross, Soumith Chintala, Gregory Chanan, Edward Yang, Zachary DeVito, Zeming Lin, Alban Desmaison, Luca Antiga, and Adam Lerer. Automatic differentiation in pytorch. 2017.
- [Peng *et al.*, 2020] Jinjia Peng, Yang Wang, Huibing Wang, Zhao Zhang, Xianping Fu, and Meng Wang. Unsupervised vehicle re-identification with progressive adaptation. In Christian Bessiere, editor, *Proceedings of the Twenty-Ninth International Joint Conference on Artificial Intelligence, IJCAI-20*, pages 913–919, 7 2020.
- [Ruan *et al.*, 2021] Dongsheng Ruan, Daiyin Wang, Yuan Zheng, Nenggan Zheng, and Min Zheng. Gaussian context transformer. In *Proceedings of the IEEE/CVF Confer-*

- ence on Computer Vision and Pattern Recognition, pages 15129–15138, 2021.
- [Vibashan *et al.*, 2023] VS Vibashan, Poojan Oza, and Vishal M Patel. Instance relation graph guided source-free domain adaptive object detection. In *2023 IEEE/CVF Conference on Computer Vision and Pattern Recognition (CVPR)*, pages 3520–3530. IEEE, 2023.
- [Wang *et al.*, 2020a] Cheng Wang, Bingpeng Ma, Hong Chang, Shiguang Shan, and Xilin Chen. Tcts: A task-consistent two-stage framework for person search. In *Proceedings of the IEEE/CVF Conference on Computer Vision and Pattern Recognition*, pages 11952–11961, 2020.
- [Wang *et al.*, 2020b] Qilong Wang, Banggu Wu, Pengfei Zhu, Peihua Li, Wangmeng Zuo, and Qinghua Hu. Ecanet: Efficient channel attention for deep convolutional neural networks. In *Proceedings of the IEEE/CVF conference on computer vision and pattern recognition*, pages 11534–11542, 2020.
- [Wang *et al.*, 2022] Yang Wang, Jinjia Peng, Huibing Wang, and Meng Wang. Progressive learning with multi-scale attention network for cross-domain vehicle re-identification. *Science China Information Sciences*, 65(6):160103, 2022.
- [Wang *et al.*, 2023] Benzhi Wang, Yang Yang, Jinlin Wu, Guo-jun Qi, and Zhen Lei. Self-similarity driven scale-invariant learning for weakly supervised person search. *arXiv preprint arXiv:2302.12986*, 2023.
- [Wang *et al.*, 2024] Yang Wang, Biao Qian, Haipeng Liu, Yong Rui, and Meng Wang. Unpacking the gap box against data-free knowledge distillation. *IEEE Transactions on Pattern Analysis and Machine Intelligence*, 2024.
- [Wang, 2021] Yang Wang. Survey on deep multi-modal data analytics: Collaboration, rivalry, and fusion. *ACM Transactions on Multimedia Computing, Communications, and Applications (TOMM)*, 17(1s):1–25, 2021.
- [Woo *et al.*, 2018] Sanghyun Woo, Jongchan Park, Joon-Young Lee, and In So Kweon. Cbam: Convolutional block attention module. In *Proceedings of the European conference on computer vision (ECCV)*, pages 3–19, 2018.
- [Xiao *et al.*, 2017] Tong Xiao, Shuang Li, Bochao Wang, Liang Lin, and Xiaogang Wang. Joint detection and identification feature learning for person search. In *Proceedings of the IEEE conference on computer vision and pattern recognition*, pages 3415–3424, 2017.
- [Xiao *et al.*, 2019] Jimin Xiao, Yanchun Xie, Tammam Tillo, Kaizhu Huang, Yunchao Wei, and Jiashi Feng. Ian: the individual aggregation network for person search. *Pattern Recognition*, 87:332–340, 2019.
- [Xu *et al.*, 2020] Chang-Dong Xu, Xing-Ran Zhao, Xin Jin, and Xiu-Shen Wei. Exploring categorical regularization for domain adaptive object detection. In *Proceedings of the IEEE/CVF Conference on Computer Vision and Pattern Recognition*, pages 11724–11733, 2020.
- [Yan *et al.*, 2019] Yichao Yan, Qiang Zhang, Bingbing Ni, Wendong Zhang, Minghao Xu, and Xiaokang Yang. Learning context graph for person search. In *Proceedings of the IEEE/CVF conference on computer vision and pattern recognition*, pages 2158–2167, 2019.
- [Yan *et al.*, 2021] Yichao Yan, Jinpeng Li, Jie Qin, Song Bai, Shengcai Liao, Li Liu, Fan Zhu, and Ling Shao. Anchor-free person search. In *Proceedings of the IEEE/CVF Conference on Computer Vision and Pattern Recognition*, pages 7690–7699, 2021.
- [Yan *et al.*, 2022] Yichao Yan, Jinpeng Li, Shengcai Liao, Jie Qin, Bingbing Ni, Ke Lu, and Xiaokang Yang. Exploring visual context for weakly supervised person search. In *Proceedings of the AAAI Conference on Artificial Intelligence*, volume 36, pages 3027–3035, 2022.
- [You *et al.*, 2019] Kaichao You, Mingsheng Long, Zhangjie Cao, Jianmin Wang, and Michael I Jordan. Universal domain adaptation. In *Proceedings of the IEEE/CVF conference on computer vision and pattern recognition*, pages 2720–2729, 2019.
- [Zhang *et al.*, 2023] Jingyi Zhang, Jiaying Huang, Zhipeng Luo, Gongjie Zhang, Xiaoqin Zhang, and Shijian Lu. Dadet: Domain adaptive detection transformer with information fusion. In *Proceedings of the IEEE/CVF Conference on Computer Vision and Pattern Recognition*, pages 23787–23798, 2023.
- [Zheng *et al.*, 2017] Liang Zheng, Hengheng Zhang, Shaoyan Sun, Manmohan Chandraker, Yi Yang, and Qi Tian. Person re-identification in the wild. In *Proceedings of the IEEE conference on computer vision and pattern recognition*, pages 1367–1376, 2017.
- [Zhong *et al.*, 2020] Yingji Zhong, Xiaoyu Wang, and Shiliang Zhang. Robust partial matching for person search in the wild. In *Proceedings of the IEEE/CVF conference on computer vision and pattern recognition*, pages 6827–6835, 2020.